Rheology of Diblock Copolymer Micellar Dispersions Having Soft Cores

Hiroshi Watanabe* and Yumi Matsumiya

Institute for Chemical Research, Kyoto University, Uji, Kyoto 611-0011, Japan

Received February 2, 2005; Revised Manuscript Received March 5, 2005

ABSTRACT: Rheological properties were examined for polybutadiene−polystyrene (PB−PS) diblock copolymer micelles that had soft PB cores and were dispersed randomly in a matrix of low-*M* homopolystyrene (hS) plasticized with dibutyl phthalate. In the linear viscoelastic regime, the micellar dispersions exhibited fast and slow relaxation processes attributed to the orientational relaxation of individual corona blocks and the relaxation of the Brownian stress (occurring through the micelle diffusion), respectively. Under large step strains, the fast and slow processes exhibited nonlinear damping in their relaxation moduli, and the damping was much stronger for the slow process than for the fast process. Under fast flow, two-step thinning of the viscosity corresponding to this damping behavior was observed. All these linear and nonlinear rheological features were quantitatively similar to those of PS−polyisoprene (PI) copolymer micelles having glassy PS cores. Analysis based on the emulsion model suggested that the interfacial relaxation of the soft PB cores of the PB−PS micelles occurred rapidly (almost together with the corona relaxation) because the PB cores had only small diameters (<40 nm). Thus, in long time scales after this interfacial relaxation, the PB core effectively behaved as a rigid core (keeping its spherical shape due to the segregation power/surface tension against the hS matrix), thereby exhibiting the above similarities with the PS−PI micelles having glassy PS cores.

1. Introduction

Diblock copolymer micelles, formed in selective solvents, have interesting rheological properties that are intimately related to spatial arrangements (distribution) of the micelles. For example, in diene-selective *n*-tetradecane, polystyrene−polybutadiene (PS−PB) and polystyrene−polyisoprene (PS−PI) diblock copolymer micelles having glassy PS cores are arranged on cubic lattices due to the osmotic interaction between the solvated diene blocks, and this lattice structure provides the systems with the plasticity (static elasticity under small strain and flow with thixotropic character under steady shear).[1−4] The plasticity is observed also for the lattice of the micelles of inverted structure, i.e., PB−PS micelles with rubbery PB cores formed in a PS-selective solvent, dibutyl phthalate.[5]

Interestingly, the plastic feature vanishes in polymeric selective solvents, homopolymers chemically identical to the micellar corona.[6−10] The homopolymer chains screen the osmotic interaction between the corona blocks, thereby allowing the micelles to be randomly dispersed and exhibit the full relaxation even under small strains in the linear viscoelastic regime. For the PS−PB and PS−PI micelles dispersed in homopolybutadiene (hB) and homopolyisoprene (hI) matrices, respectively, fast and slow relaxation processes are observed in the linear regime:[6−10] The fast process corresponds to orientational relaxation of individual corona blocks (retarded by the steric hindrance from the PS cores), while the slow process is attributed to relaxation of the Brownian stress σ_B: σ_B is a thermodynamic stress reflecting the strain-induced anisotropy in the spatial distribution of the micelles,[2,9,10] and its relaxation occurs through Stokes−Einstein diffusion of the micelles over a distance ≅ micellar core diameter.[9−12] This stress is commonly observed for random suspensions of nanoparticles exhibiting the Brownian motion.[13−18]

Corresponding to these molecular mechanisms of the fast and slow processes, the PS−PI/hI micellar dispersions exhibit characteristic nonlinear damping of their relaxation moduli under large step strains:[2,9,19] The damping seen for the fast process is similar to that of homopolymers[20−24] and attributed to retraction of the corona blocks under large strains occurring in prior to their rotational motion (orientational relaxation). The damping for the slow process, being much stronger than that for the fast process, is similar to the damping observed for random suspensions of nanosilica particles[15,16] and attributed to the nonlinearity of the Brownian stress σ_B:[9,15,16,19] Since the spatial distribution of the mutually indistinguishable particles (or micelles) becomes insensitive to the strain γ for large γ, σ_B detecting the anisotropy of this distribution does not increase in proportion to γ, thereby exhibiting the nonlinear damping. Under steady shear, two-step thinning of the viscosity corresponding to the two-step damping is observed.[25]

For the PS−PB/hB and PS−PI/hI micellar dispersions in long time scales where the corona relaxation is completed, the nonlinear rheological behavior is governed by their glassy PS cores, and one may naturally expect the above similarity with the rigid nanosilica particles. It is of interest to examine whether this similarity remains for the micellar dispersions having soft (rubbery) cores.

In relation to effects of this core softness, we remember that incompatible homopolymer blends containing micrometer-sized liquid droplets in liquid matrices exhibit a wide variety of structural changes (droplet deformation, coarsening, breakup, etc.) under large strain/fast flow[26−32] and interesting time evolution of the droplet shape, for example, evolution from cylinder to dumbbell and further to rotational ellipsoid after imposition of step strain.[26] These structural changes/shape evolution result in changes of the viscoelastic interfacial relaxation time with strain and flow rate.[27,29,31,32] It is also interesting to test whether this type of

* To whom all correspondences should be addressed. E-mail: hiroshi@scl.kyoto-u.ac.jp.

10.1021/ma050227k CCC: $30.25
Published on Web 04/02/2005

Table 1. Characteristics of Materials

code[a]	$10^{-3}M_{PB}$	$10^{-3}M_{PS}$	M_w/M_n
PB−PS copolymers			
PB−PS 26−63	26.0	63.0	1.04
PB−PS 16−81	15.5	80.6	1.05
homopolystyrene			
hS-11		10.5	1.08

[a] Sample code numbers indicate the molecular weights in unit of 1000.

nonlinearity is observed for the copolymer micellar dispersions having deformable cores.

Thus, we have examined rheological behavior of PB−PS micelles having rubbery PB cores and PS corona in a matrix of low-M homopolystyrene (hS). It turned out that the behavior of these micelles is quantitatively similar to that of PS−PI micelles having the glassy PS cores and different from that of the homopolymer blends because the micellar PB cores are very small (with the diameters < 40 nm). Details of these results are presented in this paper.

2. Experimental Section

2.1. Materials. Two polybutadiene−polystyrene (PB−PS) diblock copolymers were synthesized with butyllithium in benzene. The PB block was polymerized first, and the PS block was copolymerized after recovering a small fraction of the PB block anion as the precursor.[33a] The microstructure of PB synthesized in a similar condition is *cis*:*trans*:*vinyl* ≅ 40:50:10 (1,4-linkage:1,2-linkage ≅ 90:10).[33b]

These copolymer samples were characterized with GPC (CO-8020 and DP-8020, Tosoh Co.) equipped with refractive index (RI) and ultraviolet absorption (UV) monitors (LS-8000 and UV-8020, Tosoh Co.) connected in series. The eluent was THF, and previously synthesized monodisperse linear PB samples[34] (characterized with GPC and low-angle light scattering) were utilized as the elution standards. The PB block molecular weight M_{PB} was determined for the precursors through elution volume calibration with these standards. The PS/PB composition, giving the PS block molecular weight M_{PS}, was determined from the RI and UV signal intensities of the copolymers, with the PB block precursor and monodisperse PS samples (TSK's; Tosoh Co.) being used as the reference. Table 1 summarizes the molecular characteristics thus determined.

Rheological measurements were conducted for 15 wt % blends of the PB−PS copolymers in a matrix of low-M homopolystyrene (hS 11; obtained from Tosoh Co.) as well as for a neat hS 11 matrix. The molecular characteristics of the hS 11 sample are also shown in Table 1. The blends were plasticized with dibutyl phthalate (DBP; C_{DBP} = 24.1 wt %) so that their terminal relaxation was observed at rather low temperatures ($T \leq 75$ °C). The neat matrix was also plasticized with DBP at the same C_{DBP} (= 24.1 wt %). The blends and neat matrix were prepared by first dissolving prescribed masses of the PB−PS and hS samples and DBP (Wako Co.) in benzene at a total polymer concentration ≅ 5 wt % and then allowing benzene to thoroughly evaporate.

DBP is moderately PS-selective at around room temperature[35,36] but should be an almost common solvent for PS and PB at high T (= 65 and 75 °C where the rheological measurements were conducted). Nevertheless, microphase separation occurred for the PS−PB copolymers at these T, as revealed from rheological and scattering measurements. The volume fraction of the PB phases in the blends was estimated to be ϕ_{PB} = 0.063 (for PB−PS 26−63) and 0.035 (for PB−PS 16−81) for equal distribution of DBP to the PS and PB phases (C_{DBP} = 24.1 wt % in both phases). With such small ϕ_{PB} values, spherical micelles with PB cores and PS corona were formed in the blends.

On this equal distribution of DBP, the total concentration of the corona PS blocks and hS chains in the PS/DBP matrix phase is given by $C_{total-S} = 1 - C_{DBP}$ = 75.9 wt %, and the volume fraction of the corona blocks in the matrix phase is evaluated to be ϕ_{corona} = 0.11 and 0.13 for PB−PS 26−63 and PB−PS 16−81, respectively. Comparing of the reduced molecular weight $M_{corona}\phi_{corona}^{1.3}$ obtained from these ϕ_{corona} values with the entanglement spacing for bulk hS,[37] $M_e° = 1.8 \times 10^4$, we note that the corona PS blocks of neighboring PB−PS micelles were not entangled among themselves. The matrix hS was too short to exhibit any entanglement effect ($M_{hS} < M_e°$).

2.2. Measurements. 2.2.1. DSC Measurement. For the PB−PS/hS micellar blends and neat hS matrix quenched from 75 °C, thermal measurements were conducted with a differential scanning calorimeter (Diamond DSC, Perkin-Elmer Co.) equipped in Professor Yoko's laboratory in Institute for Chemical Research, Kyoto University. For the blends and neat hS 11 matrix, both being plasticized with DBP (C_{DBP} = 24.1 wt %), the glass transition temperatures of the PS chains therein were indistinguishable and given by T_g^{PS} = 22 °C. (This coincidence of T_g^{PS} for the blends and neat matrix was naturally expected because hS 11 was the major component in the blends.) The glass transition temperature of the PB chain ($T_g^{PB} \cong -80$ °C) was much lower than this T_g^{PS}, demonstrating the softness of the PB cores of our micelles.

2.2.2. Rheological Measurement. The blends were glassy at room temperature (≅ 15 °C < T_g^{PS} of the blends) but behaved as soft fluids at higher T to exhibit fast and slow relaxation processes. The time−temperature superposition did not work accurately for the viscoelastic data of the blends at those high T because of some changes in the equilibrium structure with T (> T_g^{PS}, T_g^{PB}). Thus, linear and nonlinear rheological measurements were conducted at fixed temperatures, T_r = 65 and 75 °C for the 15 wt % PB−PS 26−63/hS and PS−PB 16−81/hS blends, respectively, where both of the fast and slow relaxation processes were detected in our experimental window. (For comparison, the linear measurement was made also at $T > T_r$.)

The measurements were made with a laboratory rheometer (ARES, Rheometrics Co.) in a cone−plate geometry of the plate diameter = 2.5 cm and the gap angle between cone and plate = 0.1 rad. From dynamic oscillatory measurements, the linear viscoelastic storage and loss moduli, G' and G'', were obtained at various angular frequencies ω. The strain amplitude was kept small (≤0.05) in order to ensure the linearity of the G' and G'' data. The nonlinear relaxation modulus $G(t,\gamma)$ was measured against step strains of the magnitude $\gamma \leq 3$, and the non-Newtonian viscosity $\eta(\dot{\gamma})$ was obtained under steady shear at the shear rates $\dot{\gamma} \leq 5\ s^{-1}$.

Analysis of the viscoelastic data of the blends required the zero-shear viscosity $\eta_{0,matrix}$ of the neat hS 11 matrix having the total PS concentration identical to that in the matrix phase in the blends ($C_{total-S}$ = 75.9 wt % under equal distribution of DBP to the matrix and core phases). For evaluation of this $\eta_{0,matrix}$, steady flow and dynamic oscillatory tests were conducted for the neat matrix plasticized with DBP (C_{hS} = 75.9 wt %) at T_r = 65 and 75 °C.

2.2.3. SAXS measurement. For the PB−PS/hS blends charged in a cell having a mica window and quenched from T_r (= 65 and/or 75 °C) to room temperature (≅ 15 °C < T_g^{PS}), small-angle X-ray scattering (SAXS) measurements were conducted with a laboratory goniometer (RINT-2000, Rigaku Co.) equipped in Professor Kanaya's laboratory in Institute for Chemical Research, Kyoto University. The structure in the blends at T_r should have been essentially preserved on this quench. The SAXS intensity $I(q)$ was measured as a function of the magnitude of the scattering vector $q = [4\pi/\lambda] \sin(\theta/2)$, with θ and λ being the scattering angle and the X-ray wavelength (λ = 0.154 nm; Cu Kα line), respectively. Background scattering was subtracted from the measured intensity of the blends, and no further correction of the $I(q)$ data (such as the desmearing correction) was made.

3. Results and Discussion

3.1. Linear Viscoelastic Behavior. 3.1.1. Overview. Figure 1 shows angular frequency (ω) dependence

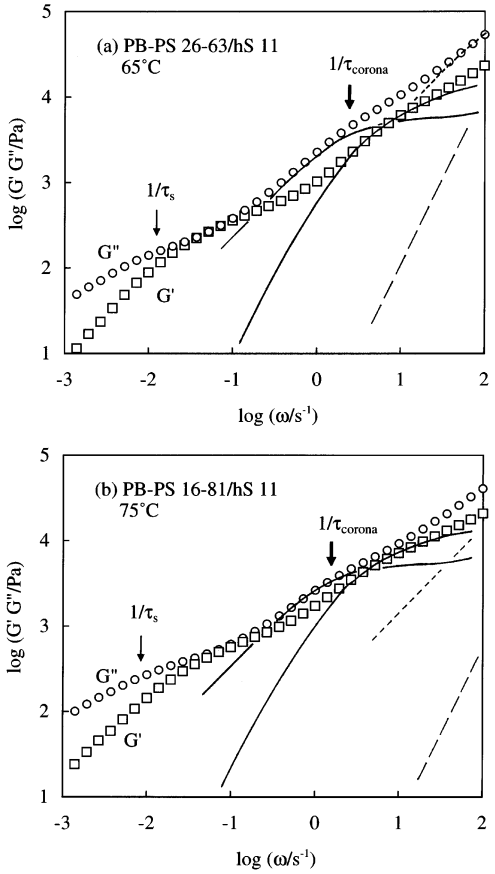

Figure 1. Linear viscoelastic behavior of the 15 wt % PB−PS 26−63/hS 11 and PB−PS 16−81/hS 11 micellar dispersions at 65 and 75 °C. These dispersions were plasticized with DBP (C_{DBP} = 24.1 wt %). Thick and thin arrows show the relaxation frequencies of the fast and slow processes of the dispersions. Dashed and dotted curves indicate G' and G'' of the neat hS 11 matrix (plasticized with DBP; C_{DBP} = 24.1 wt %) at respective temperatures, and solid curves denote G' and G'' of solution of star PS chains equivalent to the micellar corona PS blocks.

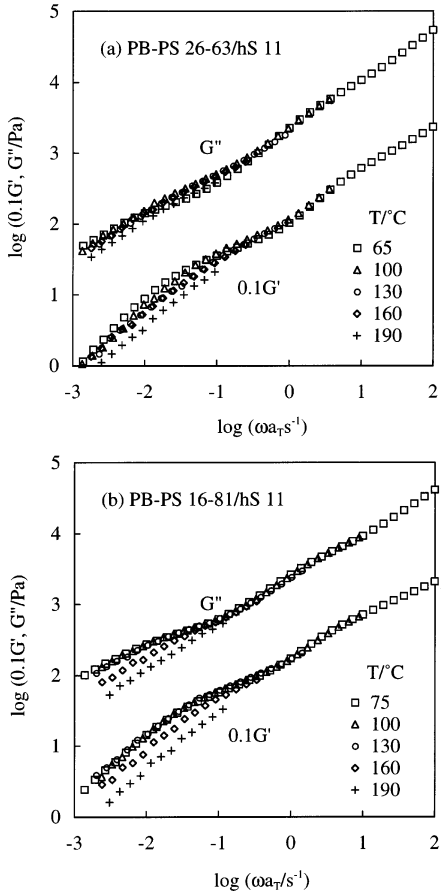

Figure 2. Test of time−temperature superposability for the 15 wt % PB−PS 26−63/hS 11 and PB−PS 16−81/hS 11 systems. The G' and G'' data of these systems at $T > T_r$ (= 65 or 75 °C) are shifted along the ω axis by a factor of a_T and best superposed onto the data at T_r in a high-ω regime. In the plots, G' data are multiplied by a factor of 0.1 to avoid heavy overlapping with the G'' data points.

of the storage and loss moduli, G' (squares) and G'' (circles), measured for the 15 wt % PB−PS 26−63/hS 11 and PB−PS 16−81/hS 11 systems at the fixed temperatures, T_r = 65 and 75 °C, respectively. The dashed and dotted curves indicate G' and G'' data of the neat hS 11 matrix (plasticized with DBP; C_{hS} = 75.9 wt %). The zero-shear viscosity of this neat matrix was

$$\eta_{0,\text{matrix}} = 760 \text{ Pa s (at 65 °C) and } 170 \text{ Pa s (at 75 °C)} \quad (1)$$

As noted in Figure 1, the PB−PS/hS systems exhibit fast and slow relaxation processes in the range of ω examined. The thick and thin arrows indicate the relaxation frequencies of these processes explained later. This two-step relaxation is similar to that observed for PS−PI and PS−PB micellar dispesions,[6−10] strongly suggesting that the microphase separation occurred in our systems to form the micelles with PB cores and PS corona at the temperatures of the rheological measurements, T_r = 65 and/or 75 °C.

The microphase separation at T_r was also examined by testing the time−temperature superposability of the data at $T \geq T_r$. In Figure 2, the G' and G'' data of the PB−PS/hS systems at $T > T_r$ are shifted along the ω axis by a factor of a_T and best superposed onto the data at T_r in a high-ω regime, as often done for bulk block copolymers.[38,39] This high-ω superposition results in a systematic decrease of the G' and G'' at low ω with increasing T. This failure of time−temperature superposition reflects changes of the microdomain structure in the PB−PS/hS systems with T ($\geq T_r$), as well-known for bulk block copolymers at T above T_g of the constituent blocks.[38,39] More importantly, the failure of the superposition indicates that our PB−PS/hS systems contained the microdomains (micelles with PB cores) at T_r. The PB and PS phases appear to be strongly segregated with each other at T_r, as judged from the fact that the above decreases of G' and G'' with T are not very large and the time−temperature superposition is roughly (not accurately) valid up 130 °C, a temperature well above T_r. (Note that a change in the structure with T and the associated failure of the superposition are not significant in the limit of strong segregation where the interaction parameter χ remains large.[39])

The micelle formation was also tested from SAXS measurements: For the PB−PS/hS systems rapidly quenched from T_r to room temperature ($\cong$ 15 °C < T_g^{PS} of the PS chains therein), Figure 3 shows the SAXS intensity $I(q)$ plotted against the magnitude of scattering vector q. The structure at T_r should have been essentially preserved on this quench. For the 15 wt % PB−PS 16−81/hS 11 system (circles), broad scattering shoulders are observed at q = 0.12 and 0.21 nm^{-1}

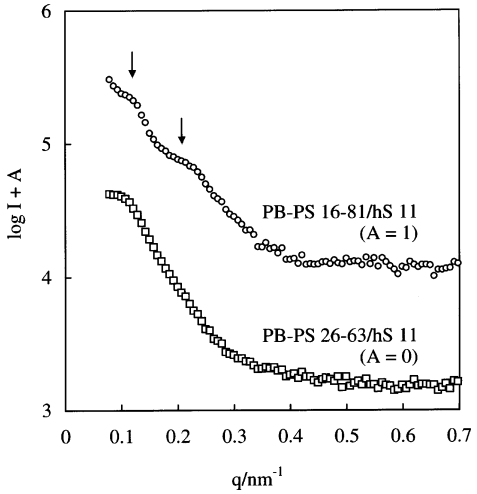

Figure 3. Semilogarithmic plots of the SAXS intensity $I(q)$ of the 15 wt % PB−PS/hS 11 systems against the magnitude of the scattering vector q. The plots for the PB−PS 16−81/hS 11 system are shifted vertically by a factor of $A = 1$ to avoid heavy overlapping with the plots for the PB−PS 26−63/hS 11 system.

(indicated with arrows). A ratio of these q values is close to that expected for the first and third interference peaks of a bcc lattice ($1:\sqrt{3}$), suggesting the formation of the spherical micelles with PB cores. (Note that the PB blocks have a small volume fraction ($\phi_{PB} = 0.035$) in the system and should form spherical domains when segregated from the PS phase.) At the same time, we should emphasize that the shoulders are very broad, and the SAXS evidence of the bcc lattice is incomplete. Namely, the lattice considered here is a significantly disordered lattice. For the 15 wt % PB−PS 26−63/hS 11 system (squares), no higher order interference shoulder is resolved, and thus no long-ranged order exists. However, the spherical micelles with the PB cores ($\phi_{PB} = 0.063$) were undoubtedly formed in this blend, as indicated by the viscoelastic data shown in Figures 1 and 2. The PB core diameter d_{core} and the micelle radius $R_{micelle}$ were estimated from the SAXS data with the method explained in Appendix:

$$\text{for PB−PS 26−63:}\quad d_{core} \cong 34\ \text{nm},\ R_{micelle} \cong 43\ \text{nm} \tag{2a}$$

$$\text{for PB−PS 16−81:}\quad d_{core} \cong 24\ \text{nm},\ R_{micelle} \cong 41\ \text{nm} \tag{2b}$$

The core scattering peak (form factor peak) for these d_{core} values, to be observed at $q_{core} = 5.765/[d_{core}/2] \cong 0.34$ and 0.48 nm^{-1} for PB−PS 26−63 and PB−PS 16−81, is not clearly detected in Figure 3 (probably because of a limited resolution of the experiment). However, those d_{core} values are consistent with the d_{core} data obtained for a similar PB−PS copolymer in DBP at low T.[5]

Thus, in the PB−PS/hS systems at T_r (= 65 and/or 75 °C), the micelles with PB cores were dispersed (almost) randomly to exhibit the full viscoelastic relaxation seen in Figure 1. In relation to this behavior, we remember that the micelles behave elastically (without exhibiting this relaxation) under a small strain when they are arranged on long-ranged lattices.[2−5] The lattice formation is driven by the osmotic interaction between the corona blocks in the low-M solvents,[1−5] and the lattice is disordered to attain the full relaxation when this interaction is screened by homopolymers chemically identical to the corona blocks.[2,6−8] In our PB−PS/hS systems, the concentrated hS chains should have well screened the osmotic interaction between the PS corona blocks, thereby disordering the lattice and allowing the micelles to exhibit the full relaxation.

3.1.2. Assignment of Fast Relaxation Mechanism. Our previous studies[2,3,9] demonstrated that the PS−PI/hI micellar dispersions having rigid PS cores exhibit fast and slow relaxation processes similar to those seen in Figure 1. The fast process had the viscoelastic mode distribution very close to that of corresponding solutions of star-branched hI chains and was assigned to the orientational relaxation of individual corona blocks.[2,3,9] We have examined whether this assignment is valid also for our PB−PS/hS micellar dispersions having the soft PB cores. The results are summarized below.

For the test of the fast relaxation mechanism, we followed the previous method[2,3,9] (based on the universality of the mode distribution of star-branched/tethered chains) to utilize the G^* data of a 60 wt % solution of a four-arm star-hS chain[40] ($M_{arm} = 76.8 \times 10^3$) in DBP and estimate G_{sol}^* of the star solutions having the arm molecular weight and concentration identical to those of the corona PS blocks of our PB−PS micelles. (At 65 and/or 75 °C, DBP should be almost equally distributed to the PS matrix and PB core, and the corona concentration in the matrix phase was evaluated to be 11 and 13 wt % for PB−PS 26−63 and PB−PS 16−81, respectively.) The solid curves in Figure 1 indicate G_{sol}' and G_{sol}'' plotted against an appropriately shifted frequency $\omega\lambda$ (λ = shift factor). These curves agree well with the G' and G'' data of the PB−PS micelles at high ω, indicating that the relaxation mode distribution of the fast process of these micelles coincides with that of the star solutions, and thus this process is attributable to the orientational relaxation of individual corona blocks. In addition, the agreement allows us to evaluate the corona relaxation time τ_{corona} in our blends from the known values of λ and the relaxation time of the stars τ_{star} as $\tau_{corona} = \tau_{star}/\lambda$. This τ_{corona} well specifies the terminal frequency of the fast process; see the thick arrows in Figure 1.

3.1.3. Assignment of Slow Relaxation Mechanism. For the slow process of the PS−PI micelles having rigid PS cores, analysis of the viscoelastic data[2,3,9] as well as diffusion experiments[10−12] demonstrated that this process is attributable to the Stokes−Einstein diffusion of the randomly dispersed micelles over a distance ≅ core diameter. For our PB−PS micelles having soft PB cores, validity of this assignment is examined below.

The viscoelastic analysis is made for the terminal relaxation time of the slow process, τ_s. This τ_s is unequivocally evaluated if the low-ω terminal tails of G' ($\propto \omega^2$) and G'' ($\propto \omega$) are experimentally detected.[9,10] However, for our PB−PS micelles not obeying the time−temperature superposition, the G' and G'' data had to be measured at the fixed temperature (T_r = 65 and/or 75 °C), and these tails were not well resolved in the range of ω examined (down to 10^{-3} s^{-1}; cf. Figure 1). Thus, τ_s of those micelles were calculated from relaxation spectra $\{g_p,\tau_p\}$ that were evaluated from the G' and G'' data at T_r: In the evaluation of the spectra, the characteristic times τ_p of the relaxation modes were set to be equally separated in the logarithmic scale (τ_p =

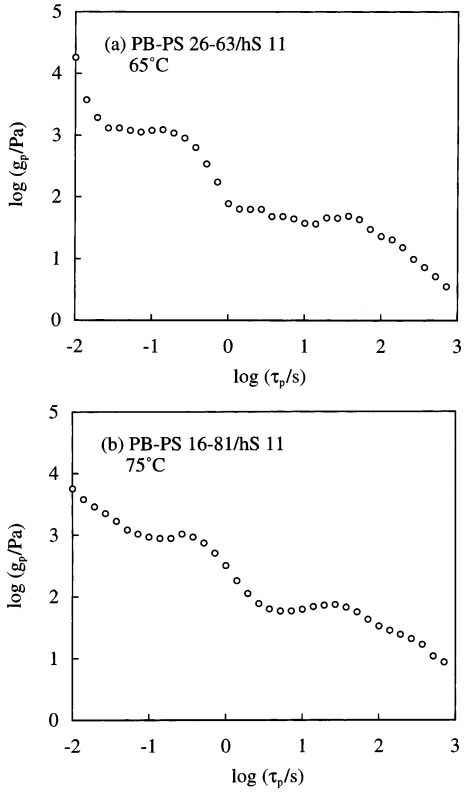

Figure 4. Viscoelastic relaxation spectra of the 15 wt % PB−PS 26−63/hS 11 and PB−PS 16−81/hS 11 systems.

$10^{-3+p/7}$ with $1 \le p \le 35$; these τ_p were identical to the reciprocal of the ω for the data points), and a previously reported iteration method[41] was utilized to determine the mode intensities g_p reproducing the data. The spectra thus evaluated are shown in Figure 4.

The fast process should be completed in the time scale for the slow process, meaning that the relaxation modes assigned to the latter process should have τ_p much longer than τ_{corona} of the former process. We assigned the modes having $\tau_p > 10\tau_{corona}$ to the slow process and evaluated τ_s as the second-moment average relaxation time:

$$\tau_s = \frac{\sum_{p \text{ for slow modes}} g_p \tau_p^2}{\sum_{p \text{ for slow modes}} g_p \tau_p} = 80 \text{ s (for PB-PS 26-63)}, \quad 120 \text{ s (for PB-PS 16-81)} \quad (3)$$

(The τ_s values did not change significantly even if the assignment of the slow modes were made with a severer criterion, $\tau_p > 30\tau_{corona}$.)

The τ_s defined by eq 3 rigorously coincides with the relaxation time $\tau_{s,tail}$ defined from the G^* terminal tails[9,10,42] if the mode times τ_p utilized in eq 3 extend well beyond $\tau_{s,tail}$. This was not the case for the τ_s values obtained above (because of the limitation of our experimental window at T_r). However, the characteristic frequency $1/\tau_s$, shown in Figure 1 with thin arrows, specifies the terminal regime of the slow process with satisfactory accuracy. Thus, we utilize the τ_s values given in eq 3 in the following analysis.

For the diffusion of the micelles over the core diameter d_{core}, two kinds of Stokes−Einstein (SE) time are defined as[9,42]

$$\tau_{SE,mat} = \pi R_{micelle} \eta_{0,matrix} d_{core}^2 / k_B T \quad (4a)$$

$$\tau_{SE,cor} = \pi R_{micelle} \eta_{0,corona} d_{core}^2 / k_B T \quad (4b)$$

Here, k_B is the Boltzmann constant, T is the absolute temperature, $R_{micelle}$ is the micelle radius, and $\eta_{0,matrix}$ and $\eta_{0,corona}$ are the zero-shear viscosities of the neat matrix and corona blocks at T_r.[43] $\tau_{SE,mat}$ and $\tau_{SE,cor}$ are the times for the SE diffusion with the matrix and corona viscosities serving as the effective viscosity η_{eff} of the medium for diffusion.

The structural parameters, d_{core} and $R_{micelle}$, were estimated from the SAXS data and summarized in eq 2. The $\eta_{0,matrix}$ data were summarized in eq 1,[43] and $\eta_{0,corona}$ was evaluated from G''_{sol} of the solution of the star chains equivalent to the corona blocks (solid curves in Figure 1):

for PB−PS 26−63 blend at 65 °C:

$$\eta_{0,corona} = 2300 \text{ Pa s} \quad (5a)$$

for PB−PS 16−81 blend at 75 °C:

$$\eta_{0,corona} = 3400 \text{ Pa s} \quad (5b)$$

In parts a and b of Figure 5, $\tau_{SE,mat}$ and $\tau_{SE,cor}$ of our PB−PS micelles calculated from these parameters are plotted against the relaxation time for the slow process τ_s given in eq 3 (unfilled symbols). The solid lines indicates relationships, $\tau_{SE,mat} = \tau_s$ (part a) and $\tau_{SE,cor} = \tau_s$ (part b).

For comparison, Figure 5 also shows the plots for the previously examined PS−PI micellar dispersions[9] with rigid PS cores (filled triangles). The plot in part a is for dilute and mutually nonentangled PS−PI micelles having the corona viscosity $\eta_{0,corona}$ comparable to/smaller than the matrix viscosity $\eta_{0,matrix}$, and the plot in part b is for concentrated and mutually entangled PS−PI micelles having $\eta_{0,corona} \gg \eta_{0,matrix}$. For the dilute and nonentangled PS−PI micelles, τ_s is close to $\tau_{SE,mat}$, and thus their slow process is attributed to the SE diffusion governed by the matrix viscosity ($\eta_{eff} = \eta_{0,matrix}$; part a).[9] In contrast, for the concentrated and mutually entangled PS−PI micelles, τ_s agrees well with $\tau_{SE,cor}$, and the slow process is attributed to the SE diffusion governed by the corona viscosity ($\eta_{eff} = \eta_{0,corona}$; part b).[9]

No intermicellar entanglement exists for our 15 wt % PB−PS 26−63 and PB−PS 16−81 micelles, as explained earlier. However, these micelles are mutually overlapping and far from the dilute limit, as noted from a fact that the micelle radius $R_{micelle}$ (eq 2) is considerably larger than a half distance between the neighboring micelles, $D/2 \cong 37$ and 32 nm for PB−PS 26−63 and PB−PS 16−81 (cf. Appendix). Correspondingly, $\eta_{0,corona}$ (eq 5) is considerably larger than $\eta_{0,matrix}$ (eq 1), in particular for PB−PS 16−81. Thus, the SE diffusion of those micelles is expected to be not governed by the neat matrix viscosity. This expectation is consistent with the results seen in Figure 5a: τ_s of our PB−PS micelles is considerably longer than $\tau_{SE,mat}$, in particular for PB−PS 16−81 (unfilled square).

For such nonentangled but deeply overlapping PB−PS micelles, the SE diffusion would be activated only after the corona relaxes and thus governed by the corona viscosity. Indeed, τ_s of these micelles agree well with $\tau_{SE,cor}$; see unfilled symbols in Figure 5b. This result strongly suggests that the slow process of the PB−PS micelles corresponds to the SE diffusion with $\eta_{eff} =$

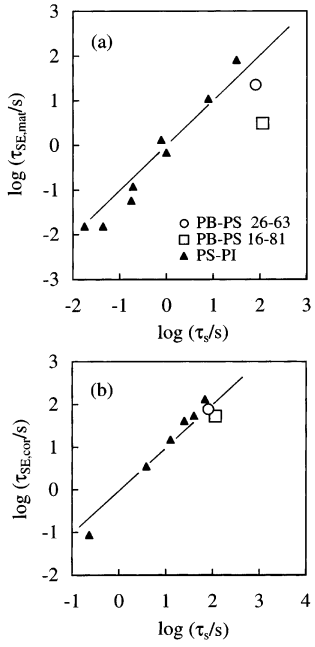

Figure 5. Plots of the SE diffusion times, (a) $\tau_{SE,mat}$ and (b) $\tau_{SE,cor}$, against the terminal relaxation time τ_s of the 15 wt % PB−PS 26−63/hS 11 and PB−PS 16−81/hS 11 micellar dispersions at 65 and 75 °C (unfilled symbols). Filled triangles indicate the plots for the previously examined PS−PI/hI micellar dispersions[9] having rigid PS cores.

$\eta_{0,corona}$. Thus, the stress of these micelles in long time scales, relaxing through this diffusion, is assigned as the Brownian stress reflecting the strain-induced anisotropy of the spatial distribution of the micelles. These features of the PB−PS micelles having the soft PB cores are identical to those of the PS−PI micelles having rigid PS cores.

3.1.4. Effect of Core Softness on Linear Relaxation Behavior. The results presented in the previous sections demonstrate that the mechanisms of the fast and slow relaxation are very similar for PB−PS and PS−PI micelles, the former having soft PB cores while the latter having rigid PS cores. In other words, the deformation of the soft PB cores, unequivocally occurring in some time scale, hardly contributes to the observed relaxation of the PB−PS micelles. For examination of effects of this core softness, the relaxation time and intensity associated with the core deformation are estimated below.

We first focus on the relaxation of individual PB blocks in the core. These blocks, tethered on the core−corona interface, may be modeled as arms of star chains. From the relaxation frequency (= $1/\eta_0 J_e$ with J_e = steady-state compliance) of bulk star PB at 25 °C reported in the literature[44] and the WLF shift factor of bulk PB,[45] the relaxation frequencies of bulk star PB chains of the arm molecular weights $M_{arm} = 26.0 \times 10^3$ and 15.5×10^3 (identical to M_{PB} of our PB blocks) were estimated to be $\omega_{star-26} \cong 50\ s^{-1}$ at 65 °C and $\omega_{star-16} \cong 800\ s^{-1}$ at 75 °C, respectively. Since the PB cores of our micelles are swollen with DBP at 65 and 75 °C, the relaxation frequencies of the PB blocks should be larger than these ω_{star}'s and out of our experimental window ($\omega \leq 100\ s^{-1}$; cf. Figure 1). In addition, the PB cores have only small volume fractions in the blends (ϕ_{core} = 0.063 and 0.035 for PB−PS 26−63 and PB−PS 16−81) and embedded in a continuous PS matrix. For these reasons, the viscoelastic response of individual PB blocks should have hardly contributed to the G^* data of our micellar dispersions at $\omega \leq 100\ s^{-1}$.

Now, we turn our attention to the interfacial relaxation of the PB cores that occurs after the relaxation of individual PB blocks. Regarding our micellar dispersions as emulsions of dilute viscous droplets (PB cores with the viscosity $\eta_{0,core}$ and volume fraction $\phi_{core} \ll 1$) in a viscous medium (corona-PS/hS matrix phase with the viscosity $\eta_{0,corona}$),[46] we may utilize the emulsion model[47−49] to estimate the interfacial relaxation time τ_{int} and relaxation intensity G_{int} as

$$\tau_{int} = \frac{\eta_{0,corona} d_{core}}{80\Gamma} \frac{(19K+16)(2K+3)}{K+1} \quad \text{with } K = \frac{\eta_{0,core}}{\eta_{0,corona}} \tag{6}$$

$$G_{int} = \frac{40\Gamma\phi_{core}}{d_{core}} \frac{1}{(2K+3)^2} \tag{7}$$

Here, Γ is the interfacial tension between the PB core and PS matrix, both being swollen with DBP.

From literature data of the viscosity of bulk star PB at 25 °C[44] and the WLF shift factor,[45] the viscosities of bulk star PB chains having $M_{arm} = 26.0 \times 10^3$ and 15.5×10^3 (= M_{PB} of our PB blocks) were estimated to be $\eta_{0,star-26} \cong 1.7 \times 10^4$ Pa s at 65 °C and $\eta_{0,star-16} \cong 1.5 \times 10^3$ Pa s at 75 °C. Since the viscosity of the swollen PB cores of our micelles should be smaller than these estimates, we can utilize the $\eta_{0,corona}$ data (eq 5) to specify a range of the viscosity ratio K (eq 6) as

$$0 < K < 7.4 \quad \text{for PB−PS 26−63 at 65 °C} \tag{8a}$$

$$0 < K < 0.44 \quad \text{for PB−PS 16−81 at 75 °C} \tag{8b}$$

No literature data were found for Γ between the swollen PB and PS phases. However, we may roughly estimate this Γ from the interfacial tension Γ_b between bulk PS and 1,2-rich PB.[50] For PS and 1,2-rich PB both having $M > 4000$, the Γ_b data at T = 140−170 °C are insensitive to M and moderately increase with decreasing T.[50] Extrapolating these data to 70 °C, we obtained $\Gamma_{b,70°C} \cong 2.5 \times 10^{-3}$ N m^{-1}. For 1,4-rich PB (= our PB block) and PS in bulk state, $\Gamma_{b,70°C}$ should have a similar value (of the order of 10^{-3} N m^{-1}) because the polarity is nearly the same for 1,4-rich and 1,2-rich PB chains.[51] For the PB core and PS matrix in our systems swollen with DBP, Γ would be significantly smaller than this $\Gamma_{b,70°C}$. Since a small amount of emulsifier (PS−PB copolymer) decreases Γ_b between bulk PS and PB phases by a factor of 10 (or more),[52,53] we assumed a similar decrease due to DBP (common solvent for PB and PS) and estimated Γ to be of the order of 10^{-4} N m^{-1}.

From the $\eta_{0,corona}$ data, the d_{core} data (eq 2), and this rough estimate of Γ ($\cong 10^{-4}$ N m^{-1} for the swollen PB cores and PS matrix), the ranges of τ_{int} and G_{int} corresponding to eq 8 are specified as

$$0.5 < \tau_{int}/s < 3.3 \text{ and } 23 < G_{int}/Pa < 820 \quad \text{for PB−PS 26−63 at 65 °C} \tag{9a}$$

$$0.5 < \tau_{int}/s < 0.7 \text{ and } 390 < G_{int}/Pa < 650 \quad \text{for PB−PS 16−81 at 75 °C} \tag{9b}$$

The maximum value of τ_{int} is associated with the minimum value of G_{int}, and vice versa.

The τ_{int} given by eq 9 is comparable to (and/or somewhat longer than) the corona relaxation time, τ_{corona} = 0.4 and 0.6 s for PB−PS 26−63 and PB−PS 16−81 (cf. thick arrows in Figure 1), but much shorter than τ_s given by eq 3. Namely, the interfacial relaxation is completed almost together with the corona relaxation before the micelle diffusion occurs. We also note that G_{int} is smaller, by a factor of ≅10 (or more), than the terminal intensity of the corona relaxation, G_{corona} = 6100 and 5000 Pa for PB−PS 26−63 and PB−PS 16−81, respectively. (G_{corona} was evaluated as a reciprocal of the steady-state compliance obtained from G_{sol}' and G_{sol}'' shown with the solid curves in Figure 1.) Because of this magnitude of G_{int} as well as the small difference between τ_{int} and τ_{corona}, the interfacial relaxation of our PB−PS micelles cannot be resolved as a separate relaxation process in the G^* data. (This interfacial relaxation gives, at best, weak broadening of the relaxation mode distribution at ω between $1/\tau_{corona}$ and $1/\tau_s$.)

As explained above, the interfacial relaxation is much faster than the micelle diffusion. This fact means that the PB cores preserve their spherical shape due to its strong segregation power (and interfacial tension) against the PS matrix and effectively behave as rigid, spherical cores in the time scale of the micelle diffusion. For this reason, the PB−PS and PS−PI micelles having different mechanical softness of the cores exhibit the similarity in their slow relaxation behavior (Figure 5b).

Here, we remember a result of rheo-SANS experiments for PEP−PEE copolymers having soft spherical domains embedded in a soft matrix:[54] Under oscillatory shear, the domains were found to deform at high frequencies but not at low frequencies where the relaxation of individual blocks was completed. This result is consistent with the above argument for our PB−PS micellar systems.

3.2. Nonlinear Relaxation Behavior. 3.2.1. Overview. For the PB−PS 26−63 and PB−PS 16−81 micellar dispersions at 65 and 75 °C, respectively, Figures 6 and 7 show the nonlinear relaxation modulus $G(t,\gamma)$ measured against step strains of the magnitude $\gamma \leq 3$. In the top and bottom panels, the $G(t,\gamma)$ data are double-logarithmically and semilogarithmically plotted against the time t. The solid curves in the top panels show the linear relaxation modulus $G(t) = \sum_p g_p \exp(-t/\tau_p)$, with $\{g_p,\tau_p\}$ being the relaxation spectrum shown in Figure 4. The thick and thin arrows indicate the relaxation times of the fast and slow processes (corona relaxation and micelle diffusion) determined in the linear regime.

The $G(t,\gamma)$ data of the micellar dispersions decrease from the linear $G(t)$ with increasing γ, and this nonlinear damping is much stronger for the slow process than for the fast process. Despite this strong damping, the relaxation time of the slow process is insensitive to the strain, as clearly noted from the semilogarithmic plots (bottom panels). Thus, the relaxation modulus for the slow process is time-strain separable and expressed as $G_s(t,\gamma) = h_s(\gamma)G_s(t)$ in its terminal regime, where $G_s(t)$ is the modulus for this process in the linear regime and $h_s(\gamma)$ is its damping function. This $h_s(\gamma)$, evaluated as a vertical shift factor required for superposing the long-t tails of the $G(t,\gamma)$ data for various γ, is later shown in Figure 10.

For a test of the nonlinearity of the fast process, we utilized the previous method[9,19] to evaluate the relaxation modulus $G_f(t,\gamma)$ for the fast process. Figure 8 shows typical results for the PB−PS 26−63 micellar dispersion under the strains γ = 0.1 and 3: At $t > 10\tau_{corona}$ where the corona relaxation should be completed, the $G(t,\gamma)$ data (unfilled symbols) were fitted with a sum of exponential terms, $G_{s,fit} = \sum_p g_p' \exp(-t/\tau_p')$; τ_p' agreed well with τ_p of the slow modes in the linear regime while g_p' decreased from the linear g_p with increasing γ. This $G_{s,fit}$ was subtracted from the data to obtain $G_f(t,\gamma)$ (filled symbols). The $G_f(t,\gamma)$ determined in this way hardly changed when the fitting was remade in a narrower range of t, $t > 20\tau_{corona}$, confirming a satisfactory accuracy of the $G_f(t,\gamma)$ data.

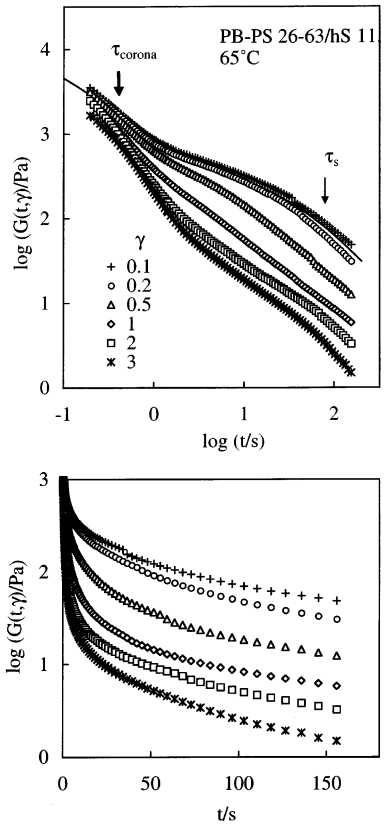

Figure 6. Double-logarithmic and semilogarithmic plots of nonlinear relaxation modulus $G(t,\gamma)$ of the 15 wt % PB−PS 26−63/hS 11 micellar dispersions at 65 °C. The solid curve in the top panel indicates the linear relaxation modulus $G(t)$ evaluated from the linear viscoelastic spectrum (Figure 4).

For the $G_f(t,\gamma)$ data thus obtained for the PB−PS 26−63 and PB−PS 16−81 micellar dispersions, Figure 9 examines validity of the time-strain separability. The solid curves indicates the linear relaxation modulus $G_{sol}(t)$ of the solutions of star chains equivalent to the micellar corona blocks. (This $G_{sol}(t)$ was evaluated from the G_{sol}' and G_{sol}'' of these solutions shown with the solid curves in Figure 1.) The $G_f(t,\gamma)$ data for $\gamma \leq 0.5$ were very close to this $G_{sol}(t)$ while the data decreased from $G_{sol}(t)$ with increasing $\gamma \geq 1$. Thus, in Figure 9, the $G_f(t,\gamma)$ data for γ = 0.1 are utilized as the linear relaxation modulus $G_f(t)$ for the fast process, and the data for larger γ are normalized by an appropriately chosen damping function $h_f(\gamma)$ to achieve the best superposition on this linear $G_f(t)$ at long t. Excellent superposition seen here demonstrates validity of the time-strain separability for the fast process; $G_f(t,\gamma) = h_f(\gamma)G_f(t)$ in the terminal regime of this process. The $h_f(\gamma)$ data thus determined are later shown in Figure 10.

3.2.2. Similarity with Rigid-Core Micelles and Difference from Soft-Phase Blends. The PS−PI

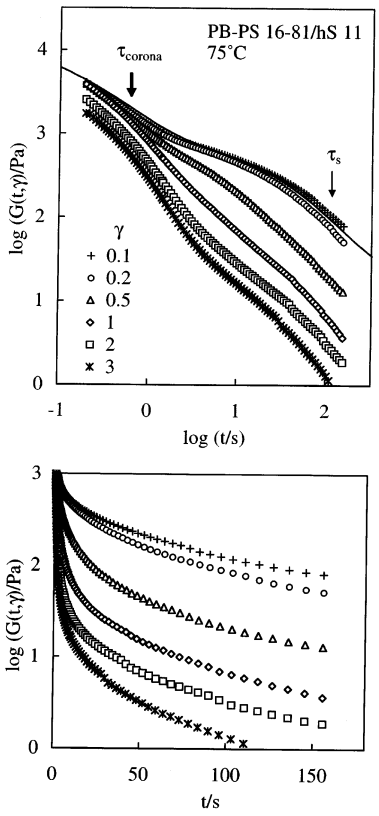

Figure 7. Double-logarithmic and semilogarithmic plots of nonlinear relaxation modulus $G(t,\gamma)$ of the 15 wt % PB−PS 16−81/hS 11 micellar dispersions at 75 °C. The solid curve in the top panel indicates the linear relaxation modulus $G(t)$ evaluated from the linear viscoelastic spectrum (Figure 4).

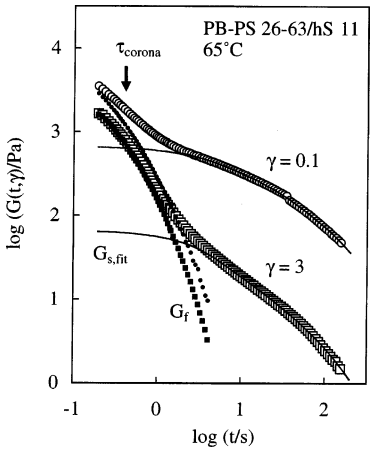

Figure 8. Separation of the $G(t,\gamma)$ data of the 15 wt % PB−PS 26−63/hS 11 micellar dispersion into the moduli $G_f(t,\gamma)$ and $G_s(t,\gamma)$ for the fast and slow relaxation processes. The results are shown for $\gamma = 0.1$ (in the linear regime) and $\gamma = 3$ (in the nonlinear regime).

micelles having rigid PS cores satisfy the time-strain separability for both of their fast and slow processes.[2,9,19] In this sense, the nonlinear feature is qualitatively similar for those micelles and our PB−PS micelles having soft PB cores. As a quantitative test of this similarity, Figure 10 compares the damping functions of our PB−PS micelles (large unfilled symbols) with those obtained for representative PS−PI micellar dispersions in nonentangling hI matrices[9,19] (filled symbols). These micelles are neither entangled among themselves nor with the matrix chains. Small unfilled circles and triangles indicate the $h(\gamma)$ data for en-

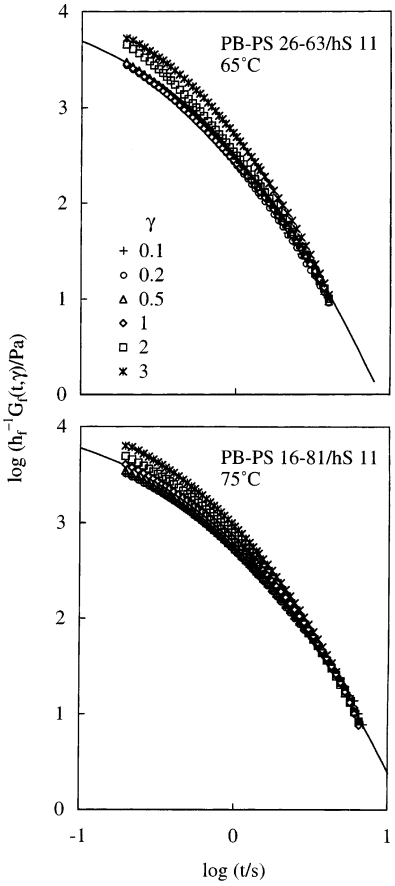

Figure 9. Comparison of the normalized relaxation moduli $h_f^{-1}G_f(t,\gamma)$ ($\gamma = 0.1-3$) for the fast process of the 15 wt % PB−PS 26−63/hS 11 and PB−PS 16−81/hS 11 micellar dispersions.

tangled[20,21] and nonentangled[22] homopolystyrene (hS) solutions.

In Figure 10a, we note that the $h_f(\gamma)$ data for the fast process (corona relaxation) are indistinguishable for the PB−PS and PS−PI micelles having soft PB and rigid PS cores, respectively, and are close to the $h(\gamma)$ data of hS chains. This result demonstrates that the damping of this process is similar to that for the homopolymers and attributable to the retraction of the strain-elongated corona blocks occurring in prior to their rotational motion (orientational relaxation), as fully discussed previously.[9,19]

In relation to this point, we also note that the $h_f(\gamma)$ data of the mutually nonentangled micelles are close to but a little smaller than the $h(\gamma)$ data of nonentangled homopolymers. For the PS−PI micelles having rigid PS cores, this small difference is partly attributable to the filler effect from the rigid core that increases a local strain in the corona phase to enhance the damping.[9] However, for the PB−PS micelles having soft PB cores, this filler effect does not seem to be significant because the PB cores should be deformed on application of step strain. Instead, the deformed cores would recover its spherical shape in a time scale of the corona relaxation, as explained earlier. This shape recovery activates motion of the PS corona ends (anchored on the PB core), and this end motion may enhance the corona retraction/damping, thereby contributing partly to the small difference between $h_f(\gamma)$ of the PB−PS micelles and $h(\gamma)$ of the nonentangled homopolymers. This coupling between the shape recovery (interfacial relaxation) and

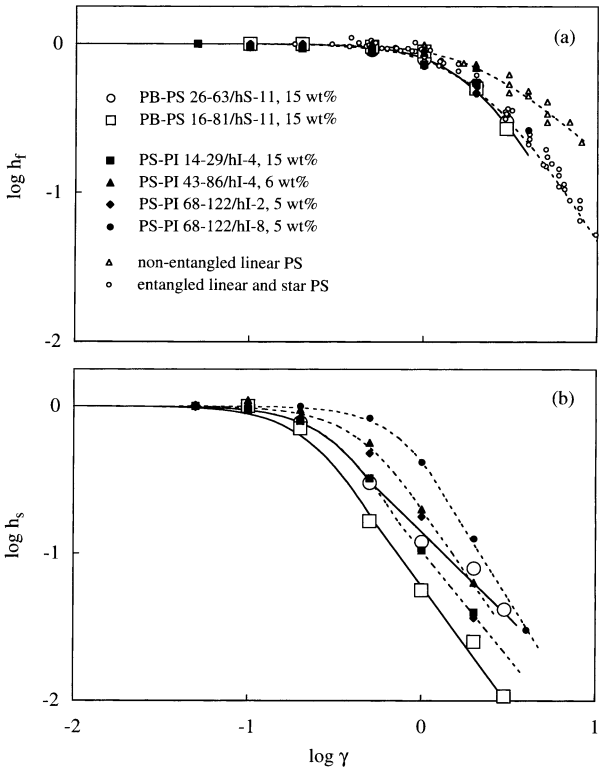

Figure 10. Damping functions $h_f(\gamma)$ and $h_s(\gamma)$ for the fast and slow processes of the 15 wt % PB−PS/hS 11 micellar dispersions (large unfilled symbols). For comparison, the data are also shown for PS−PI micellar dispersions having rigid PS cores[9,19] (filled symbols) and for homopolystyrene solutions[20−22] (small unfilled symbols). In both (a) and (b), the dotted curves are for guide of eye, and the solid curves represent the empirical fitting functions for h_f and h_s utilized in the BKZ calculation of viscosity (Figure 11): for PB−PS 26−63, $h_f = [1 + 0.25\gamma^{2.1}]^{-1}$ and $h_s = [1 + 10\gamma^{2.2}]^{-1}$ ($\gamma < 0.513$), $h_s = 0.14\gamma^{-1.15}$ ($\gamma > 0.513$); for PB−PS 16−81, $h_f = [1 + 0.25\gamma^{2.1}]^{-1}$ and $h_s = [1 + 20\gamma^{2.2}]^{-1}$ ($\gamma < 0.525$), $h_s = 0.06\gamma^{-1.6}$ ($\gamma > 0.525$).

corona retraction is still hypothetical and is to be examined in more details in future work. However, irrespective of the details of this coupling, we should note, as the most important feature, that the nonlinear damping of the corona relaxation is indistinguishable for our PB−PS and PS−PI micelles and not significantly affected by the core softness.

Now, we turn our attention to $h_s(\gamma)$ data for the slow process. For the PS−PI micelles having the glassy PS cores, $h_s(\gamma)$ strongly decreases with γ, and this decrease is enhanced with increasing micelle concentration,[9,19] as shown for the representative data in Figure 10b (filled symbols). This behavior is similar to that of random suspensions of Brownian particles, and indeed, the γ dependence of $h_s(\gamma)$ is in quantitative agreement with that of the $h(\gamma)$ data of the Brownian suspensions,[15,16] as demonstrated previously.[9,19] The $h_s(\gamma)$ data for the PB−PS micelles having soft PB cores (unfilled symbols) agree with the data for the PS−PI micelles and thus exhibit this similarity with the Brownian suspensions. From this result, the nonlinear damping of the slow process of the PB−PS micelles is attributed to the micelle distribution anisotropy (the structural origin of the Brownian stress) that becomes insensitive to γ for large γ, as fully discussed for the PS−PI micelles[9,19] and Brownian suspensions.[15,16]

Here, we should emphasize that the PB cores of the PB−PS micelles should have preserved their spherical

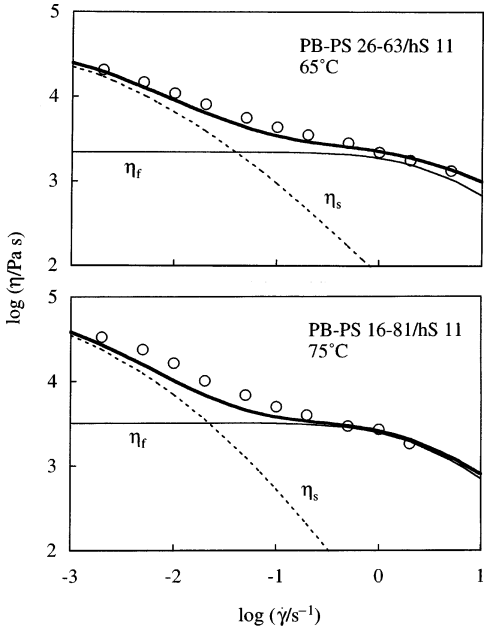

Figure 11. Steady-state viscosity η measured for the 15 wt % PB−PS 26−63/hS 11 and PB−PS 16−81/hS 11 micellar dispersions at 65 and 75 °C (circles). The thick solid curves denote η_{BKZ} calculated from the BKZ constitutive equation utilizing the nonlinear damping data, and the thin solid and dotted curves indicate the viscosities η_f and η_s calculated for the fast and slow processes, respectively.

shape and effectively behaved as rigid cores in the time scale of micelle diffusion, as discussed for the linear G^* data. This feature naturally leads to the similarity of the nonlinearity at long t seen for the PB−PS and PS−PI micelles having the soft PB and rigid PS cores.

In relation to this feature of the PB core, a comment needs to be made for emulsion-type homopolymer blends having micrometer-sized liquid droplet phases in liquid matrices. In the linear regime, the blends exhibit the interfacial relaxation as the terminal viscoelastic relaxation.[27,29,31,32,49,55] On imposition of a large strain, the spherical droplet is deformed almost affinely to become a flattened object. This flattened shape evolves to rod, dumbbell, and rotational ellipsoid with time (if the droplet is not pinched into smaller droplets), and finally the spherical shape is recovered.[26−28] Corresponding to this complicated change in the droplet shape, the terminal interfacial relaxation under step strains is retarded by a factor of ≅10 with increasing strain up to $\gamma = 3$;[27,29] i.e., the time-strain separation severely fails for the emulsion-type blends.

The PB−PS micellar dispersions satisfy the time-strain separability and behave quite differently from the emulsion-type homopolymer blends. The PB cores in these dispersions are quite small (cf. eq 2) so that their interfacial relaxation is much faster than the micelle diffusion, as discussed earlier. For this reason, some retardation of the interfacial relaxation with γ, even if it occurs, is fully masked by the time-strain separable micelle diffusion process and not detected in the viscoelastic experiments. In other words, the huge difference in the sizes of the PB cores in our micellar dispersions and droplets in the emulsion-type blends results in the above difference.

3.3. Non-Newtonian Flow Behavior. Figure 11 shows the steady-state viscosity of the PB−PS 26−63 and PB−PS 16−81 micellar dispersions at 65 and 75 °C (circles). Both dispersions exhibit two-step thin-

ning behavior that is very similar to the behavior observed for PS−PI micellar dispersions having rigid PS cores.[9,25]

For the PS−PI micelles, the viscosity was satisfactorily described by the BKZ constitutive equation utilizing the data for the nonlinear damping functions $h_f(\gamma)$ and $h_s(\gamma)$:[9,25]

$$\eta_{BKZ}(\dot{\gamma}) = \phi_{matrix}\eta_{0,matrix} + \eta_f(\dot{\gamma}) + \eta_s(\dot{\gamma}) \quad (10)$$

with

$$\eta_x(\dot{\gamma}) = -\int_0^\infty \frac{dG_x(t)}{dt} h_x(\gamma_t)t\, dt \quad (x = f, s) \quad (11)$$

Here, ϕ_{matrix} is the volume fraction of the matrix hS 11 in the system, and γ_t (= $\dot{\gamma}t$) represents a strain in an interval of time from 0 to t imposed through the flow at the rate $\dot{\gamma}$.

We utilized the $h_f(\gamma)$ and $h_s(\gamma)$ data for our PS−PB micelles (Figure 10) in eq 11 to calculate the viscosity of these micelles and examined the validity of the BKZ equation. (Empirical fitting functions for h_f and h_s, shown with solid curves in Figure 10, were utilized in this calculation.) In Figure 11, the thin solid and dotted curves indicate η_f and η_s calculated from eq 11, and the thick solid curves denote the BKZ viscosity η_{BKZ} (eq 10). The η data are close to this η_{BKZ}, suggesting that the two-step thinning of the PB−PS micelles is attributed to the large deformation of the corona (leading to the thinning of η_f) and the $\dot{\gamma}$ insensitivity of the micelle distribution anisotropy (giving the thinning of η_s), as similar to the situation for the PS−PI micelles having rigid PS cores.[9,25] This similarity is again related to the rapid interfacial relaxation of the soft PB cores of the PB−PS micelles, as discussed for the nonlinear damping under step strains.

For the emulsion-type homopolymer blends containing micrometer-sized liquid droplet phases, a wide variety of structural changes (such as breakup and coarsening) are observed under fast flow.[30−32] The relaxation time after cessation of shear flow changes with the shear rate[31,32] because of these structural changes under flow (as well as the complicated time evolution of the droplet shape after cessation of flow).

In contrast, our PS−PB micelles exhibited no similar change in the relaxation time: As demonstrated in Figure 12, the viscosity decay function $\eta_-(t,\dot{\gamma})$ (= decaying stress normalized by $\dot{\gamma}$) of these micelles after cessation of steady shear has a $\dot{\gamma}$-insensitive terminal relaxation time. This lack of the change in the relaxation time is again related to the very rapid shape recovery (interfacial relaxation) of the small PB cores as well as to lack of the core disruption/pinching during the flow. In other words, the difference between the steady flow behavior of the emulsion-type homopolymer blends and our PB−PS micellar dispersions reflects a huge difference in the sizes of the droplets in the blends and the micellar PB cores and the thermodynamic stabilization of the PB cores.

4. Concluding Remarks

We have examined rheological behavior of PB−PS micelles that had soft PB cores and were randomly dispersed in the low-M hS matrix. In the linear viscoelastic regime, the micelles exhibited fast and slow processes attributable to the orientational relaxation of individual corona PS blocks and the relaxation of the Brownian stress (occurring through the micelle diffusion over a distance ≅ core diameter). Under large step strains, the fast and slow processes exhibited nonlinear damping similar to that for homopolymer solutions and Brownian suspensions, respectively. Under fast flow, two-step thinning corresponding to this damping behavior was observed.

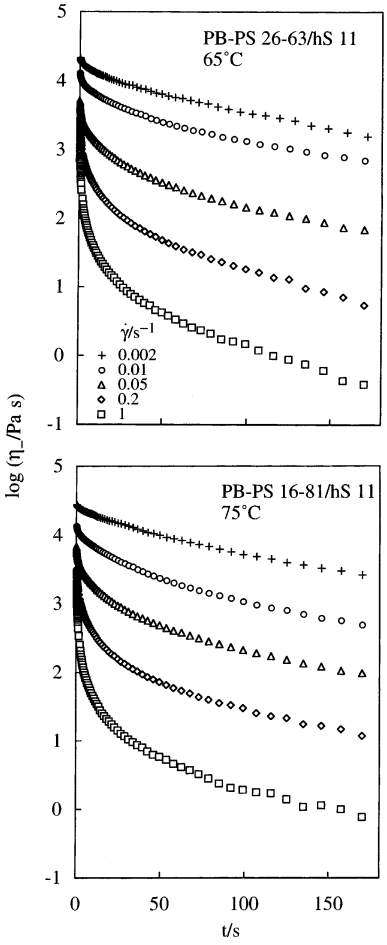

Figure 12. Viscosity decay function $\eta_-(t,\dot{\gamma})$ measured for the 15 wt % PB−PS 26−63/hS 11 and PB−PS 16−81/hS 11 micellar dispersions at 65 and 75 °C. The $\eta_-(t,\dot{\gamma})$ data are semilogarithmically plotted against time after cessation of steady shear.

All above features of the PB−PS micelles having soft PB cores were similar to those of PS−PI micelles having rigid PS cores. Analysis based on the emulsion model suggested that the interfacial relaxation of the PB cores occurred almost together with the corona relaxation and was much faster than the micelle diffusion because the PB cores have only small diameter (= O(10 nm)). Thus, the PB cores preserved their spherical shape and effectively behaved as rigid cores in the time scale of the diffusion, thereby exhibiting this similarity. For the same reason, the PB−PS micelles exhibited no changes in the terminal relaxation time under large strains and after cessation of fast flow, thereby distinguishing themselves from the emulsion-type homopolymer blends that have micrometer-sized droplet phases and exhibit changes in the relaxation time.

Acknowledgment. Discussion with Professor D. Vlassopoulos at FORTH, Institute for Electronic Structure & Laser, was very helpful for the authors to begin

this study. The authors thank Mr. T. Konishi at Professor T. Kanaya's lab, ICR, Kyoto University, for his help for SAXS measurements and Mr. H. Masai and Ms. M. Mizuno at Professor T. Yoko's lab, ICR, Kyoto University, for their help for DSC measurements.

Appendix. Estimation of Core Diameter d_{core} and Micelle Radius $R_{micelle}$

As seen in Figure 3, the PB−PS 16−81 micelles exhibit the SAXS profile with a very broad but bcc-like character. Although the SAXS evidence for the bcc lattice is incomplete (i.e., the lattice is highly disordered), we assumed the bcc relationship for the average distance D between neighboring micelles and scattering vector q_1 (= 0.12 nm^{-1}) for the first order shoulder, $D = 2\pi\sqrt{3/2}q_1^{-1}$ (≅ 64 nm), to estimate the number density ν_{core} of the PB cores. From this density, $\nu_{core} = 3\sqrt{3}D^{-3}/4 \cong 4.9 \times 10^{21}$ m^{-3}, and the number of PB blocks per unit volume of the blend, $\nu_{PB} = 9.9 \times 10^{23}$ m^{-3} (evaluated from the blend density, the copolymer concentration and the block molecular weights), the number of PB blocks per core was estimated to be $n_{PB} = \nu_{PB}/\nu_{core} \cong 200$. On the equal distribution of DBP to the PS and PB phases at 75 °C (resulting in the PB concentration of 75.9 wt % in the core), the PB core is swollen with DBP to a volumetric swelling ratio of $Q = 1.28$. Then, the core diameter is estimated to be $d_{core} = 2\{3Qn_{PB}m_{PB}/4\pi\rho_{PB}\}^{1/3} \cong 24$ nm (m_{PB} = mass of a PB block and ρ_{PB} = bulk density of PB). This d_{core} value is consistent with that determined for a micellar lattice of a similar copolymer ($M_{PB} = 13.3 \times 10^3$, $M_{PS} = 53.9 \times 10^3$, and $C_{PB-PS} = 28$ wt %) formed in DBP;[5] $d_{core} = 18.2$ nm in the nonswollen state, lending support to our estimate of d_{core} for the PB−PS 16−81 micelle.

For the PB−PS 26−63 micelle, no higher order interference shoulder is clearly resolved, and d_{core} cannot be estimated with the above method based on the assumption of broad bcc-like character. Thus, we utilized the two-thirds power-law relationship between the spherical domain size and block molecular weight established for the strongly segregated copolymers[56] to estimate $d_{core,26-63}$ for PB 26−63 from the above $d_{core,16-81}$ value and the molecular weight ratio r (= 26.0/15.8) of the PB blocks of the two copolymers. The result was $d_{core,26-63} = r^{2/3}d_{core,16-81} \cong 34$ nm. The average intermicellar distance corresponding to this $d_{core,26-63}$ is $D \cong 74$ nm.

Now, we turn our attention to the micelle radius $R_{micelle}$. In the concentrated matrix, the excluded-volume effect should be screened and $R_{micelle}$ can estimated as $0.5d_{core} + 2^{1/2}R_{PS,\theta}$, where $R_{PS,\theta}$ is the unperturbed end-to-end distance of the PS block (corona block) and the factor of $2^{1/2}$ accounts for expansion of the corona blocks due to the steric repulsion[3,7,9,57] from the PB core (having d_{core} comparable to $R_{PS,\theta}$). With an empirical relationship[58] between $R_{PS,\theta}$ and M_{PS} and the above d_{core} values, $R_{micelle}$ was estimated to be ≅43 nm and ≅41 nm for the PB−PS 26−63 and PB−PS 16−81 micelles, respectively.

References and Notes

(1) Watanabe, H.; Kotaka, T.; Hashimoto, T.; Shibayama, M.; Kawai, H. *J. Rheol.* **1982**, *26*, 153.
(2) Watanabe, H. *Acta Polym.* **1997**, *48*, 215.
(3) Sato, T.; Watanabe, H.; Osaki, K.; Yao, M. L. *Macromolecules* **1996**, *29*, 3881.
(4) Watanabe, H.; Kanaya, T.; Takahashi, Y. *Macromolecules* **2001**, *34*, 662.
(5) Watanabe, H.; Matsumiya, Y.; Kanaya, T.; Takahashi, Y. *Macromolecules* **2001**, *34*, 6742.
(6) Watanabe, H.; Kotaka, T. *J. Rheol.* **1983**, *27*, 223.
(7) Watanabe, H.; Sato, T.; Osaki, H. *Macromolecules* **1996**, *29*, 104.
(8) Watanabe, H.; Sato, T.; Osaki, H. *Macromolecules* **1996**, *29*, 113.
(9) Matsumiya, Y.; Watanabe, H. *Macromolecules* **2004**, *37*, 9861.
(10) Watanabe, H.; Sato, T.; Osaki, K.; Hamersky, M. W.; Chapman, B. R.; Lodge, T. *Macromolecules* **1998**, *31*, 3740.
(11) Gohr, K.; Pakula, T.; Tsutsumi, K.; Schartl, W. *Macromolecules* **1999**, *32*, 7156.
(12) Gohr, K.; Schartl, W. *Macromolecules* **2000**, *33*, 2129.
(13) Mellema, J.; van der Werff, J. C.; Blom, C.; de Kruif, C. G. *Phys. Rev. A* **1989**, *39*, 3696.
(14) Shikata, T.; Pearson, D. S. *J. Rheol.* **1994**, *38*, 601.
(15) Watanabe, H.; Yao, M. L.; Yamagishi, A.; Osaki, K.; Shikata, T.; Niwa, H.; Morishima, Y. *Rheol. Acta* **1996**, *35*, 433.
(16) Watanabe, H.; Yao, M. L.; Osaki, K.; Shikata, T.; Niwa, H.; Morishima, Y. *Rheol. Acta* **1999**, *38*, 2.
(17) Brady, J. F. *J. Chem. Phys.* **1993**, *99*, 567.
(18) Bender, J. W.; Wagner, N. J. *J. Colloid Interface Sci.* **1995**, *172*, 171.
(19) Watanabe, H.; Sato, T.; Osaki, K.; Yao, M. L. *Macromolecules* **1996**, *29*, 3890.
(20) Osaki, K.; Nishizawa, K.; Kurata, M. *Macromolecules* **1982**, *15*, 1068.
(21) Osaki, K.; Takatori, E.; Kurata, M.; Watanabe, H.; Yoshida, H.; Kotaka, T. *Macromolecules* **1990**, *23*, 4392.
(22) Takatori, E.; Osaki, K.; Kurata, M.; Hirayama, T. *Nihon Reoroji Gakkaishi (J. Soc. Rheol. Jpn.)* **1988**, *16*, 99.
(23) Fetters, L. J.; Kiss, A. D.; Pearson, D. S.; Quack, G. F.; Vitus, F. J. *Macromolecules* **1993**, *26*, 647.
(24) Watanabe, H. *Prog. Polym. Sci.* **1999**, *24*, 1253.
(25) Watanabe, H.; Yao, M. L.; Sato, T.; Osaki, K. *Macromolecules* **1997**, *30*, 5905.
(26) Yamane, H.; Takahashi, M.; Hayashi, R.; Okamoto, K.; Kashihara, H.; Masuda, T. *J. Rheol.* **1998**, *42*, 567.
(27) Okamoto, K.; Takahashi, M.; Yamane, H.; Kashihara, H.; Watanabe, H.; Masuda, T. *J. Rheol.* **1999**, *43*, 951.
(28) Hayashi, R.; Takahashi, M.; Yamane, H.; Jinnnai, H.; Watanabe, H. *Polymer* **2001**, *42*, 757.
(29) Okamoto, K.; Takahashi, M.; Watanabe, H.; Koyama, K.; Masuda, T. Stress Relaxation of Polyisobutylene/Polydimethylsiloxane Blends under Large Step Strain and Calculation of Stress from Droplet Shape. In *Advanced Polymers and Processing (Proceedings of ICAPP 2001 Yonezawa)*; Iwakura, K., Ed.; City Print: Yonezawa, Japan, 2002; p 195.
(30) Wetzel, E. D.; Tucker, C. L. *J. Fluid Mech.* **2001**, *426*, 199.
(31) Tucker, C. L.; Moldenaers, P. *Annu. Rev. Fluid Mech.* **2002**, *34*, 177.
(32) Jansseune, T.; Moldenaers, P.; Mewis, J. *Rheol. Acta* **2004**, *43*, 592.
(33) (a) The PB block of one of the copolymer, PB−PS 16−81, was made with deutrated monomer for a future neutron scattering experiment under shear. (b) Morton, M. *Anionic Polymerization: Principles and Practice*; Academic Press: New York, 1983.
(34) Watanabe, H.; Urakawa, O.; Yamada, H.; Yao, M. L. *Macromolecules* **1996**, *29*, 755.
(35) Lodge, T. P.; Xu, X.; Ryu, C. Y.; Hamley, I. W.; Fairclough, J. P. A.; Ryan, A. J.; Pedersen, J. S. *Macromolecules* **1996**, *29*, 5955.
(36) Hanley, K. J.; Lodge, T. P.; Huang, C. I. *Macromolecules* **2000**, *33*, 5918.
(37) Ferry, J. D. *Viscoelastic Properties of Polymers,* 3rd ed.; Wiley: New York, 1980.
(38) Bates, F. S.; Rosedale, J. H.; Fredrickson, G. H. *J. Chem. Phys.* **1990**, *92*, 6255.
(39) Bates, F. S.; Fredrickson, G. H. *Annu. Rev. Phys. Chem.* **1990**, *41*, 525.
(40) Watanabe, H.; Yoshida, H.; Kotaka, T. *Macromolecules* **1992**, *25*, 2442.
(41) Watanabe, H.; Matsumiya, Y.; Inoue, T. *Macromolecules* **2002**, *35*, 2339.
(42) Watanabe, H. *Kobunshi Ronbunshu* **2001**, *58*, 135.
(43) The viscosities of the neat matrix and corona blocks, $\eta_{0,matrix}$ and $\eta_{0,corona}$, are to be evaluated in the isomonomeric friction (iso-ζ) state. Since our PS−PB/hS blends and neat hS 11 matrix contained the same amount (24.1 wt %) of DBP and

had the same T_g^{PS}, the viscosities at the same temperature (T_r) were utilized as the viscosities in the iso-ζ state.
(44) Raju, V. R.; Menezes, E. V.; Marin, G.; Graessley. W. W.; Fetters, L. J. *Macromolecules* **1981**, *14*, 1668.
(45) Colby, R. H.; Fetters, L. J.; Graessley, W. W. *Macromolecules* **1987**, *20*, 2226.
(46) Since the corona viscosity $\eta_{0,corona}$ is considerably larger than the matrix viscosity $\eta_{0,matrix}$ and the interfacial relaxation of the PB cores can be completed only after the corona relaxation, we may utilize $\eta_{0,corona}$ as the medium viscosity in the emulsion model.
(47) Choi, S. J.; Schowalter, W. R. *Phys. Fluids* **1975**, *18*, 420.
(48) Palierne, J. F. *Rheol. Acta* **1990**, *29*, 204.
(49) Graebling, D.; Muller, R.; Palierne, J. F. *Macromolecules* **1993**, *26*, 320.
(50) Nam, K. H.; Jo, W. H. *Polymer* **1995**, *36*, 3727.
(51) Wu, S. In *Surface and Interfacial Tensions of Polymers, Oligomers, Plasticizers, and Organic Pigments*, in *Polymer Handbook*; Brandrup, J., Immergut, E. H., Eds.; Wiley: New York, 1989.
(52) Anastasiadis, S. H.; Gancarz, I.; Koberstein, J. T. *Macromolecules* **1989**, *22*, 1449.
(53) Park, D. W.; Roe, R. J. *Macromolecules* **1991**, *24*, 5324.
(54) Koppi, K. A.; Tirrell, M.; Bates, F. S.; Almdal, K.; Mortensen, K. *J. Rheol.* **1994**, *38*, 999.
(55) In homopolymer blends containing micrometer-sized droplets, the droplet diffusion should occur after the interfacial relaxation. However, the number density of such large droplets is quite small (compared to that of the copolymer micelles examined in this study) so that the viscoelastic intensity associated to the droplet diffusion is too small to be detected experimentally.
(56) Hashimoto, T.; Fujimura, M.; Kawai, H. *Macromolecules* **1980**, *13*, 1660.
(57) Dimarzio, E. A. *J. Chem. Phys.* **1965**, *42*, 2101.
(58) Miyaki, Y.; Einaga, Y.; Fujita, H. *Macromolecules* **1978**, *11*, 1180.

MA050227K